Nanoscale

Accepted Manuscript

This article can be cited before page numbers have been issued, to do this please use: L. Kong, X. Liu, J. J. Wei, S. Wang, B. Xu, D. Long and F. Chen, *Nanoscale*, 2018, DOI: 10.1039/C8NR03495H.

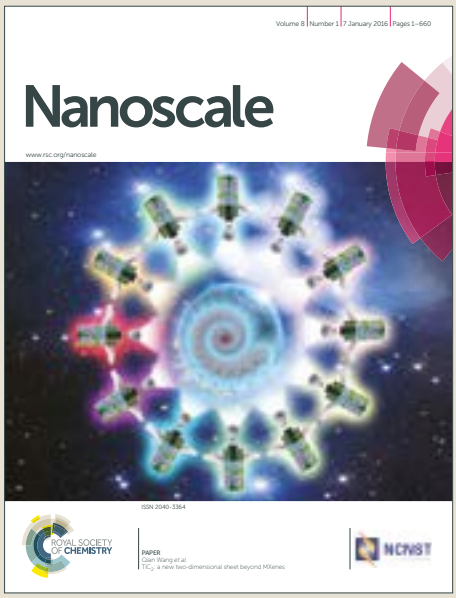

This is an Accepted Manuscript, which has been through the Royal Society of Chemistry peer review process and has been accepted for publication.

Accepted Manuscripts are published online shortly after acceptance, before technical editing, formatting and proof reading. Using this free service, authors can make their results available to the community, in citable form, before we publish the edited article. We will replace this Accepted Manuscript with the edited and formatted Advance Article as soon as it is available.

You can find more information about Accepted Manuscripts in the author guidelines.

Please note that technical editing may introduce minor changes to the text and/or graphics, which may alter content. The journal's standard Terms & Conditions and the ethical guidelines, outlined in our author and reviewer resource centre, still apply. In no event shall the Royal Society of Chemistry be held responsible for any errors or omissions in this Accepted Manuscript or any consequences arising from the use of any information it contains.

View Article Online
DOI: 10.1039/C8NR03495H

Journal Name

ARTICLE

T-Nb_2O_5 nanoparticle enabled pseudocapacitance with a fast Li-ion intercalation

Received 00th January 20xx,
Accepted 00th January 20xx

DOI: 10.1039/x0xx00000x

www.rsc.org/

Lingping Kong[a], Xiaoteng Liu[b], Jinjia Wei[a], Steven Wang[c], Ben Bin Xu[b]*, Donghui Long[d]*, Fei Chen[ab]*

Orthorhombic Nb_2O_5 (*T*-Nb_2O_5) nanocrystallites are successfully fabricated through evaporation induced self-assembly (EISA) method guided by a commericalised triblock copolymer – Pluronic F127. We demonstrate a morphology transition of *T*-Nb_2O_5 from continuous porous nanofilm to monodisperse nanoparticle by changing the content of Pluronic F127. The electrochemical results show that the optimized monodisperse of Nb-2 with particle size of 20 nm achieve premier Li-ion intercalation kinetics and higher rate capability than mesoporous *T*-Nb_2O_5 nanofilms. Nb-2 present an initial intercalation capacity of 528 and 451 C g^{-1} at current densities of 0.5 and 5 A g^{-1} and performed stable capacity of 499 C g^{-1} after 300 charge/discharge cycles and 380 C g^{-1} after 1000 cycles, respectively. We would expect this copolymer guided monodispersing of *T*-Nb_2O_5 nanoparticles with high Li^+ intercalation performance to open up new window for novel EES technologies.

Introduction

Recently, the research on high performance electrochemical energy storage (EES) has achieved significant progresses by innovating pseudocapacitive materials, i.e. transition metal oxides [1-4]. Faradaic charge storage in transition metal oxides enables high power density and high energy density through a fast sequence of reversible faradaic redox, electrosorption or intercalation processes at the surface or near-surface region of electrodes [5,6]. Unlike traditional battery materials, the charge/discharge processes in pseudocapacitors are not dominated by ion diffusion, thus, charge storage can occur on the order of seconds and minutes. The latest research trend in high performance pseudocapacitive materials is to design novel materials with the short path length and high active-surface area by controlling the nano-morphologies [7-13].

Orthorhombic Nb_2O_5 (*T*-Nb_2O_5), a typical pseudocapacitive material, holds a unique property of reversible Li-ion intercalation reaction, $Nb_2O_5 + xLi^+ + xe^- \leftrightarrow Li_xNb_2O_5$, where a maximum capacity of charge storage can be reached at 728 C g^{-1} when *x* is 2 [3]. *T*-Nb_2O_5 has attracted considerable interests for its high theoretical specific capacity, fast Li-ion intercalation kinetics and reversible lithiation/delithiation process [14-18]. Some strategies have been proposed to synthesis Nb_2O_5 with desired morphologies, aiming to optimise the electrochemical properties [19-23]. Brezesinski *et al*. synthesized ordered mesoporous *T*-Nb_2O_5 thin films and achieved significant enhancement in capacitive energy storage [24]. Liu and his co-worker fabricated Nb_2O_5 nanosheets through hydrothermal reaction, and obtained high rate Li-ion storage performance with the Nb_2O_5 nanosheets [25]. Zhou *et al*. used Nb_2O_5 nanobelts as lithium intercalation electrode and showed high reversible capacity, high rate capability and excellent cycling stability [26].

The low dimensional *T*-Nb_2O_5 structure brings advantages that can facilitate electrolyte ions and electrons transfer, offer high surface area with abundant active sites and sustain the crystal structure for durable charge/discharge process. However, challenge remains to develop a facile and sustainable method to prepare *T*-Nb_2O_5 nanocrystals and controllably form the desired morphologies, and use it to improve charge storage capacity for EES.

In this paper, we propose a facile process - evaporation induced self-assembly (EISA) guided by triblock copolymers - Pluronic F127 (a.k.a F127), to fabricate *T*-Nb_2O_5 nanostructure. Different crystalline size and morphology can be achieved by tuning the weight ratio of F127 from 0.5 to 2, a phase transition from mesoporous nanofilms to monodisperse nanoparticles will be demonstrated. We also discover that the monodisperse *T*-Nb_2O_5 nanoparticles exhibited faster Li-ion intercalation kinetics and higher rate capacity than continuous mesoporous *T*-Nb_2O_5 nanofilms with the similar crystallite size. This finding could bring new concept for novel Nb_2O_5 electrodes with fast Li-ion intercalation by introducing monodisperse nanoparticles.

Results and discussion

Structural and morphological characterization

The schematic of EISA process and structure measurement by XRD are presented in Fig. 1. The inorganic $NbCl_5$ and guiding agent F127 nucleation firstly reacted (Fig. 1a) to form O-Nb–O bridges, accompanied by an aqueous sol-gel process. An organic-inorganic

[a] School of Chemical Engineering and Technology, Xi'an Jiaotong University, Xi'an 710049, China
[b] Smart Materials and Surfaces Laboratory, Faculty of Engineering and Environment, Northumbria University, Newcastle upon Tyne NE1 8ST, UK
[c] School of Chemical Engineering and Advanced Materials, Newcastle University, Newcastle Upon Tyne, Tyne and Wear NE1 7RU, UK
[d] State Key Laboratory of Chemical Engineering, East China University of Science and Technology, Shanghai 200237, China
Electronic Supplementary Information (ESI) available: [details of any supplementary information available should be included here]. See DOI: 10.1039/x0xx00000x

View Article Online
DOI: 10.1039/C8NR03495H

hybrid structure was generated by the following aggregation of $NbCl_5$/F127 micelles. Finally, the amorphous Nb_2O_5 crystallizes were transited into orthorhombic structure when we annealed the Nb/F127 precursor films at 600 °C. The particle size and morphology of *T*-Nb_2O_5 can be directly regulated by controlling the amount of F127. The weight ratios of F127 to Nb_2O_5 were designed as 0.5:1, 1:1, 1.5:1 and 2:1, with the samples named as Nb-0.5, Nb-1, Nb-1.5 and Nb-2, correspondingly.

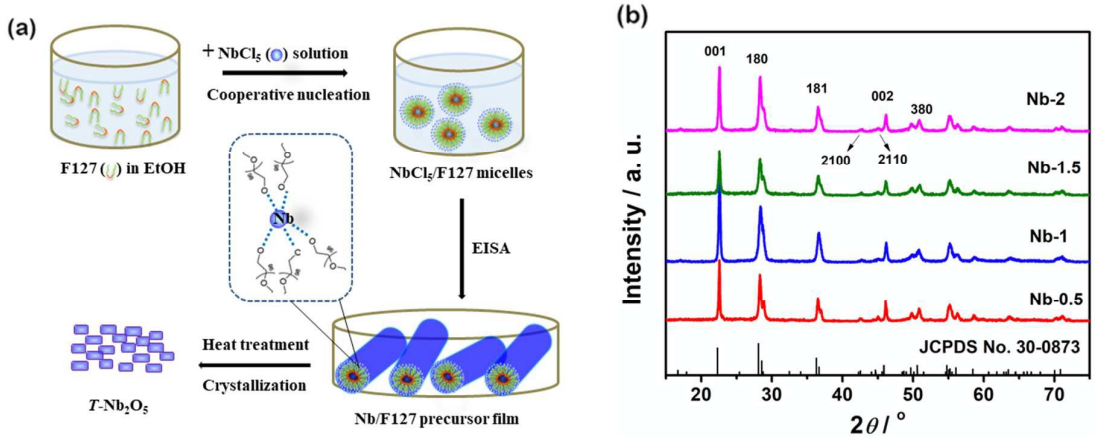

Fig 1. (a) schematic of synthesis process and (b) XRD results for all samples

The XRD results in Fig. 1b, suggest a highly crystalline with an orthorhombic unit cell, which can be indexed to the JCPDS No. 30-0873, i.e. the diffraction peaks centred at 22.6, 28.4, 36.6, 42.8, 45.0, 46.2, and 50.9 ° can be indexed as (001), (180), (181), (2100), (2110), (002), and (380) reflections of *T*-Nb_2O_5. The XRD results also reveal a decrease of average crystallite size due to the increase on F127, which agrees well to the predicted results obtained from Scherrer's equation (Table S1). We use TGA and DSC to verify the component ratios of F127 to Nb_2O_5 in weight (Fig. S1) and find that there is a slight weight loss from 50 to 200 °C due to the removal of residual water and solvent as well as the oxidation of some remained organic groups. Between 200 °C to 350 °C, the F127 decomposes thoroughly. An exothermic peak appears beyond 400 °C, indicating the rearrangement of crystal structure. XPS spectrum of the Nb-2 in Fig. S2 presented two peaks, $Nb3d_{5/2}$ at 207.00 eV and $Nb3d_{3/2}$ at 209.75 eV, which are in good agreement with the binding energies of Nb_2O_5.

The porosity properties for samples were assessed by N_2 adsorption-desorption isotherms, the pore size distribution data is shown in Fig. S3. These isotherms present very similar type IV isotherms with a hysteresis loop at P/P_0 of 0.8-1, suggesting a coexistence of mesopores and macropores. With increasing the amount of F127, the specific surface area and the average mesoporous diameters are increased, which also lead to more active edge surface. More porosity data are provided in Table S1.

We next study the morphology of *T*-Nb_2O_5 as a function of the weight ratio of F127 to Nb_2O_5. SEM observations in Fig. 2a - 2d revealed that particle size decreases with increasing amount of F127, the overall morphology is very different from the Nb_2O_5 without F127 (Fig. S4). By adding the F127, the morphology starts with continuous mesoporous nanofilms (Nb-0.5, Nb-1, and Nb-1.5), then transits into monodispersed nanoparticles (Nb-2). From the TEM images of Nb-0.5 (Fig. 2e) and Nb-2 (Fig. 2f), we find that the Nb-2 has a smaller size of around 20 nm with disordered particle-overlapped structure. The HR-TEM image in Fig. 2f (insert), unveils

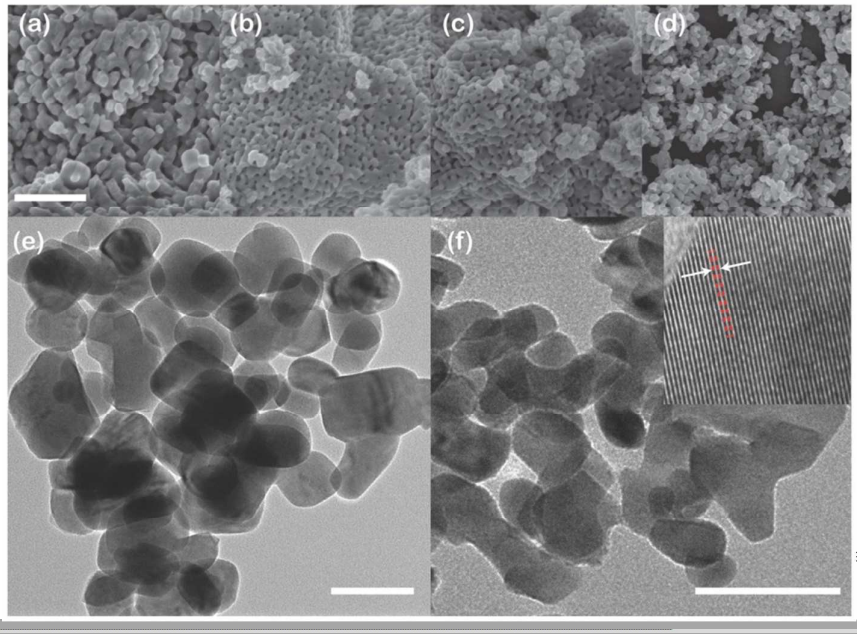

Fig. 2. SEM observations of (a) Nb-0.5, (b) Nb-1, (c) Nb-1.5 and (d) Nb-2, the scale bars are 500 nm; TEM results of (e) Nb-0.5 and (f) Nb-2, the scale bars are 50 nm

View Article Online
DOI: 10.1039/C8NR03495H

the (001) plane (lattice parameter of 3.90 Å) in the Nb-2 nanocrystals corresponding with orthorhombic structure.

Electrochemical characterization

The cyclic voltammogram (CV) results at various sweep rates are presented in Fig. 3a-d. At low sweep rate, all CVs show symmetric anodic and cathodic peaks with ignorable voltage separation. This means fast and reversible Li-ion interactions occurred within *T*-Nb_2O_5 ($Nb_2O_5 + xLi^+ + xe^- = Li_xNb_2O_5$, 0 < x < 2). Moreover, the Nb-1.5 and Nb-2 at 1 mV s^{-1} show two cathodic peaks at around 1.45 V and 1.75 V, respectively. However, Nb-0.5 and Nb-1 exhibit only one broad cathodic peak around 1.45 V. Our hypothesis is that additional intercalation active sites occur in Nb-1.5 and Nb-2, due to their smaller crystalline size and more specific surface area that enable fast Li^+ transportation. Among all CV results, the potential region of 2-3 V makes minor contributions to the total capacity. While this region expands the operating potential widow, thus greatly improves the total energy density according to the equation: $E = \frac{1}{2} C_s \Delta V^2$.

We next study the relationship between capacity and sweep rate to furtherly understand the Li-ion intercalation. The plots of specific capacity *vs* $v^{-1/2}$ in Fig. 3f show two distinct regions. In region 1 (*v* < 20 mV s^{-1}), the specific capacity is mostly independent of the sweep rate, which means charge storage mainly arising from capacitive process. In region 2 (*v* > 20 mV s^{-1}), the specific capacity decreases quickly with *v*, indicating that charge storage is mainly controlled by diffusion process. After comparing galvanostatic charge-discharge (GCD) curves for all samples at a current density of 1 A g^{-1} (Fig. 4a), we discover that *T*-Nb_2O_5 undergoes highly reversible Li^+ intercalation reaction by showing symmetric slope curves. The initial specific capacity of Nb-2 reaches the highest value as 521 C g^{-1} at 1 A g^{-1}. Nb-2 also has the best rate capability (Fig. 4b) with a slight decrease in the capacitance as current density increases. At a high current density of 20 A g^{-1}, the Nb-2 can still deliver a reasonable high capacity of 250 C g^{-1}. Moreover, Nyquist plot of Nb-2 in Fig. S5 shows a high phase-angle impedance property and a low faradic charge transfer resistance which accelerated the fast Li-ion intercalation.

The kinetic mechanism of Li^+ insertion/extraction reaction was investigated from the relation between sweep rate and capacity or current, where can be expressed as $i = av^b$. When the value of *b* is 0.5, the current is controlled by diffusion process. When b is 1, it means that Li-ion intercalation process is capacitive behaviour. By scaling log(*i*) *versus* log(*v*) of cathodic peaks, the value of *b* can be calculated in Fig. 3e. It is found that the *b* value for Nb-2 is 1 corresponding to a typical capacitive intercalation. We found that the Nb-1.5 has a *b*-value of 0.9 which is lower than Nb-2. Combining with SEM and TEM results, these results indicate that Li^+ insertion/extraction kinetics in Nb-2 monodisperse nanoparticles are more efficient than Nb-1.5 continuous mesoporous films. The continuous mesoporous Nb-0.5 films with 45 nm particle size has a *b*-value of 0.85, which means that the charge storage arriving from both semi-infinite diffusion and capacitive processes.

The high rate capability of *T*-Nb_2O_5 implies that the crystal structure allows exceptionally rapid ionic and electronic transportations. This result suggests that the intercalation induced pseudocapacitance and rate ability of *T*-Nb_2O_5 strongly depend on the specific surface area and particle size, rather than the continuous mesoporous film structure.

The durability of the materials was assessed by cyclic testing at current densities of 0.5 A g^{-1} and 5 A g^{-1}, the results are shown in Fig. 4c and 4d. The capacitance results have a slight attenuation after 300 cycles at 0.5 A g^{-1} (Fig. 4c), which represents a highly

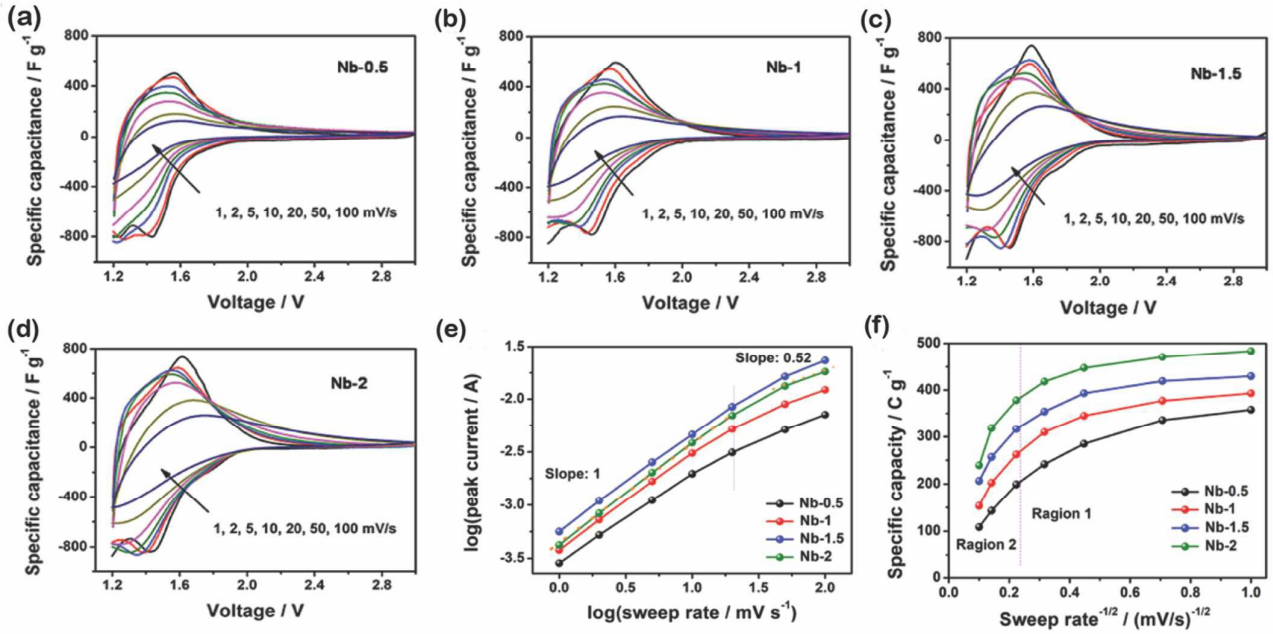

Fig. 3. CV curves of (a) Nb-0.5, (b) Nb-1, (C) Nb-1.5 and (d) Nb-2 at increasing scan rate at room temperature in 3-limbed cell; (e) Plot of specific capacity *vs* $v^{-1/2}$ and (f) *b*-value determination of the peak cathodic currents. Electrochemical tests were performed at room temperature using three-electrode

View Article Online
DOI: 10.1039/C8NR03495H

reversible Li^+ insertion/extraction into/from *T*-Nb_2O_5 enabled by the highly crystalline of *T*-Nb_2O_5. At 0.5 A g^{-1}, the Nb-2 shows an initial capacity of 528 C g^{-1}, with low capacity fading ~5.5% (499 C g^{-1}) at the end of the 300th cycle. At 5 A g^{-1}, the Nb-2 still shows the highest initial capacity of 451 C g^{-1} and 380 C g^{-1} at the end of the 1000th cycle, which is ~25% more than that of Nb-1.5 and 250% of that for Nb-0.5.

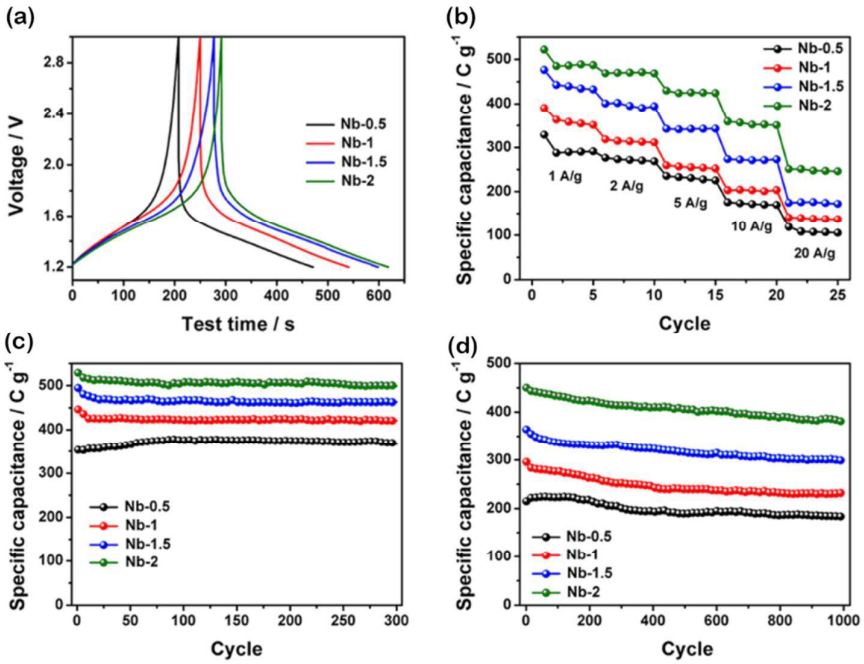

Fig. 4. (a) GCD curves, (b) rate capability and (c, d) cyclic performances for all samples

Conclusions

We fabricated *T*-Nb_2O_5 nanomaterials through evaporation induced self-assembly (EISA) method, two different morphologies have been achieved as monodisperse and continuous mesoporous nanofilms, which can be controllably formed by changing the addition of a triblock copolymer - F127. With this configurable microstructure, excellent electrochemical performances were achieved as a result of the unique orthorhomobic crystal structure in our Nb-2 materials. For the optimized Nb-2 with monodisperse structure and 20 nm particle size, electrochemical results show faster Li^+ intercalation kinetics, good high-rate capability with a capacity of 250 C g^{-1} at 20 A g^{-1}, and excellent cycling performance which the specific capacity is from 528 to 499 C g^{-1} after 300 cycles at 0.5 A g^{-1} and from 451 to 380 C g^{-1} after 1000 cycles at 5 A g^{-1}. We anticipate that the discovery of this new structure-property relationship in *T*-Nb_2O_5 nanomaterials will shed a light on novel high performance EES.

Experimental Section

Materials synthesis

The orthorhombic *T*-Nb_2O_5 crystallite was synthesized through evaporation induced self-assembly (EISA) process. Briefly, 1.2 g $NbCl_5$ powder (Sigma-Aldrich) was dissolved in 20 mL dry ethanol immersed in ice bath, and a certain amount of F127 (Sigma-Aldrich) was dissolved in another 20 ml ethanol with 0.5 mL deionized water. Once these solutions are uniformly mixed, $NbCl_5$ alcohol solution was then added drop-wisely into the F127 solution. The mixed solution was stirred in an ice bath for 1 h in order to prevent uncontrolled hydrolysis. The homogeneous mixture was then slowly poured into the Petri dishes. After slow evaporation at room temperature for 24 h, the precursor Nb/F127 films were obtained. Finally, the precursor films were thermos-annealed at 600 °C for 2 h at room temperature to obtain Nb_2O_5 nanocrystals with orthorhombic structure.

Materials characterization

The crystalline structure was characterized by a powder X-ray diffraction (XRD) at 40 kV and 100 mA with Cu Kα radiation (λ=1.5406 Å). The morphology was observed by scanning electron microscopy (SEM，FEI-300) and transmission electron microscopy (TEM, JEOL 2100F). The amount of F127 in the samples was confirmed by thermogravimetric analysis (TGA). The specific surface area and pore structure of samples were determined by N_2 adsorption–desorption isotherms at 77 K after being degassed under vacuum at 433 K for 6 h. The Brunauer-Emmett-Teller (BET) method was utilized to calculate the specific surface areas. The total pore volume was calculated using a single point. The pore size distributions were derived from the desorption branch using the Barrett-Joyner-Halenda (BJH) model.

Electrochemical measurements

Nb_2O_5 electrodes were prepared by mixing the active material, carbon black (Timcal Super C65) and polyvinylidene fluoride (PVdF) binder in an 8:1:1 weight ratio in N-methyl-2-pyrrolidinone (NMP). The homogeneous slurry was then coated onto 20 μm Cu current collectors. After drying at 100 °C for 12 hours, coated composite electrodes were pressed into 12-mm diameter using stainless steel roller. Electrochemical tests were performed using three-electrode system with the obtained material as working electrode, lithium foil as reference electrode, commercial activated carbons (Maxsorb II)

View Article Online
DOI: 10.1039/C8NR03495H

as counter electrode, Celgard 2400 microporous film as the separator, and 1 M $LiPF_6$ (EC/DMC/DEC=1:1:1 in volume ratio) as electrolyte. A potential window of 1.2-3 V was chosen in this work, to investigate the electrochemical performance induced by Li-ion intercalation, since there no redox peaks were found in the range of 0.8-1.2 V (vs. Li+/Li) in our background tests. All electrochemical tests were performed at room temperature. Both the current density and specific capacitance were calculated based on the weight of active Nb_2O_5.

Conflicts of interest

There are no conflicts to declare.

Acknowledgements

This work is financially supported by National Science Foundation of China (No. 51636006), Shanghai Rising Star Program (15QA1401300) and the Engineering and Physical Sciences Research Council (EPSRC) grants - EP/N007921/1 and EP/P026435/1.

References

1 P. Simon and Y. Gogotsi, *Nat. Mater.*, 2008, **7**, 845-854.
2 P. Simon, Y. Gogotsi and B. Dunn, *Science*, 2014, **343**, 1210-1211.
3 V. Augustyn, J. Come, M.A. Lowe, J.W. Kim, P.L. Taberna, S.H. Tolbert, H.D. Abruña, P. Simon and B. Dunn, *Nat. Mater.*, 2013, **12**, 518-522.
4 Y. Jiang, M. Hu, D. Zhang, T. Yuan, W. Sun, B. Xu and M. Yan, *Nano Energy*, 2014, **5**, 60-66.
5 B.E. Conway and W.G. Pell, *J. Solid State Electrochem.*, 2003, **7**, 637-644.
6 B. E. Conway, *J. Electrochem. Soc.*, 1991, **138**, 1539-1548.
7 A. S. Arico, P. Bruce, B. Scrosati, J. M. Tarascon and W. V. Schalkwijk, *Nat. Mater.*, 2005, **4**, 366-377.
8 P. Poizot, S. Laruelle, S. Grugeon, L. Dupont and J. M. Tarascon, *Nature*, 2000, **407**, 496-499.
9 X. L. Wang, G. Li, Z. Chen, V. Augustyn, X. M. Ma, G. Wang, B. Dunn and Y. F. Lu, *Adv. Energy Mater.*, 2011, **1**, 1089-1093.
10 L. F. Nazar, G. Goward, F. Leroux, M. Duncan, H. Huang, T. Kerr and J. Gaubicher, *Int. J. Inorg. Mater*, 2001, **3**, 191-200.
11 V. Augustyn, P. Simon and B. Dunn, *Energ. Environ. Sci.,* 2014, **7**, 1597-1614.
12 T. Yuan, Y. Jiang, W. Sun, B. Xiang, Y. Li, M. Yan, B. Xu, S. Dou, *Adv. Func. Mater.,* 2016, **26**, 2198-2206.
13 Y. Jiang, Y. Li, W. Sun, W. Huang, J. B. Liu, B. Xu, C. Jin, T. Ma, C. Wu, M. Yan, *Energ. Environ. Sci.*, 2015, **8**, 1471-1479.
14 A. A. Lubimtsev, P. R. C. Kent, B. G. Sumpter, P. Ganesh *J. Mater. Chem. A,* 2013, **1**, 14951-14956.
15 L. Kong, C. Zhang, S. Zhang, J. Wang, R. Cai, C. Lv, W. Qiao, L. Ling, D. Long, *J. Mater. Chem. A*, 2014, **2**, 17962-17970.
16 J. W. Kim, V. Augustyn and B. Dunn, *Adv. Energy Mater.*, 2012, **2**, 141-148.
17 J. Come, V. Augustyn, J. Woung Kim, P. Rozier, P. L. Taberna, P. Gogotsi, J. W. Long, B. Dunn and P. Simon, *J. Electrochem. Soc.,* 2014, **161**, A718-A725.
18 L. Kong, C. Zhang, J. Wang, W. Qiao, L. Ling and D. Long, *ACS Nano*, 2015, **9**, 11200-11208.
19 C. H. Lai, D. Ashby, M. Moz, Y. Gogotsi, L. Pilon and B. Dunn, *Langmuir*, 2017, **33**, 9407-9415.
20 L. Kong, C. Zhang, J. Wang, W. Qiao, L. Ling and D. Long, *Sci. Rep-UK*, 2016, **6**, 1-10.
21 J. Zhang, H. Chen, X. Sun, X. Kang, Y. Zhang, C. Xu, Y. Zhang, *J. Electrochem. Soc.*,2017,**164**, A820-A825.
22 L. Kong, X. Cao, J. Wang, W. Qiao, L. Ling, D. Long, *J. Power Sources*, 2016,**309**,42-49.
23 X. Liu, X. Wu, K. Scoot, *Catal. Sci. Technol.,* 2014,**4**,3891-3898.
24 K. Brezesinski, J. Wang, J. Haetge, C. Reitz, S.O. Steinmueller, S.H. Tolbert, B.M. Smarsly, B. Dunn, T. Brezesinski, *J. Am. Chem. Soc.*,2010,**132**,6982-6990.
25 M. Liu, C. Yan, Y. Zhang, *Sci. Rep-UK*, 2015,**5**,8326.
26 M. Wei, K. Wei, M. Lchihara, H. Zhou, *Electrochem. Commun.*,2008,**10**,980-983.